Electronic Supplementary Information

Atomically-Dispersed Cobalt Ions on Polyphenol-Derived Nanocarbon Layers to Improve Charge Separation, Hole Storage, and Catalytic Activity of Water-Oxidation Photoanodes

Yuri Choi,‡[ab] Sanghyun Bae,‡[ab] Byeong-Su Kim[c] and Jungki Ryu*[ab]*

[a]Department of Energy Engineering, School of Energy and Chemical Engineering, Ulsan National Institute of Science and Technology (UNIST), Ulsan 44919, Republic of Korea

[b]Emergent Hydrogen Technology R&D Center, Ulsan National Institute of Science and Technology (UNIST), Ulsan 44919, Republic of Korea

[c]Department of Chemistry, Yonsei University, Seoul 03722, Republic of Korea

‡These authors contributed equally to this work.

E-mail: jryu@unist.ac.kr (J.R); bskim19@yonsei.ac.kr (B.-S.K)

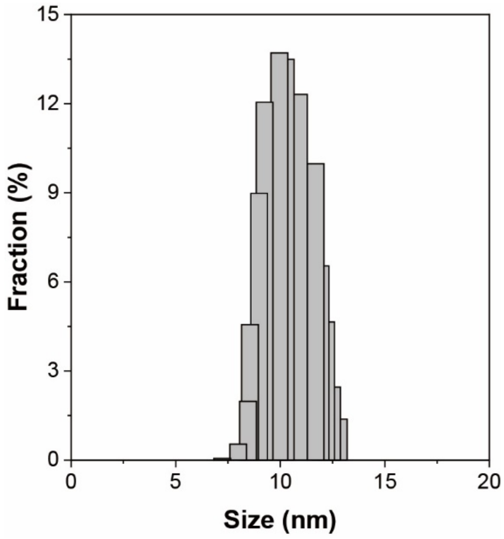

Fig. S1 Dynamic light scattering of N-TAGQDs. The average N-TAGQD size was 10.5 nm.

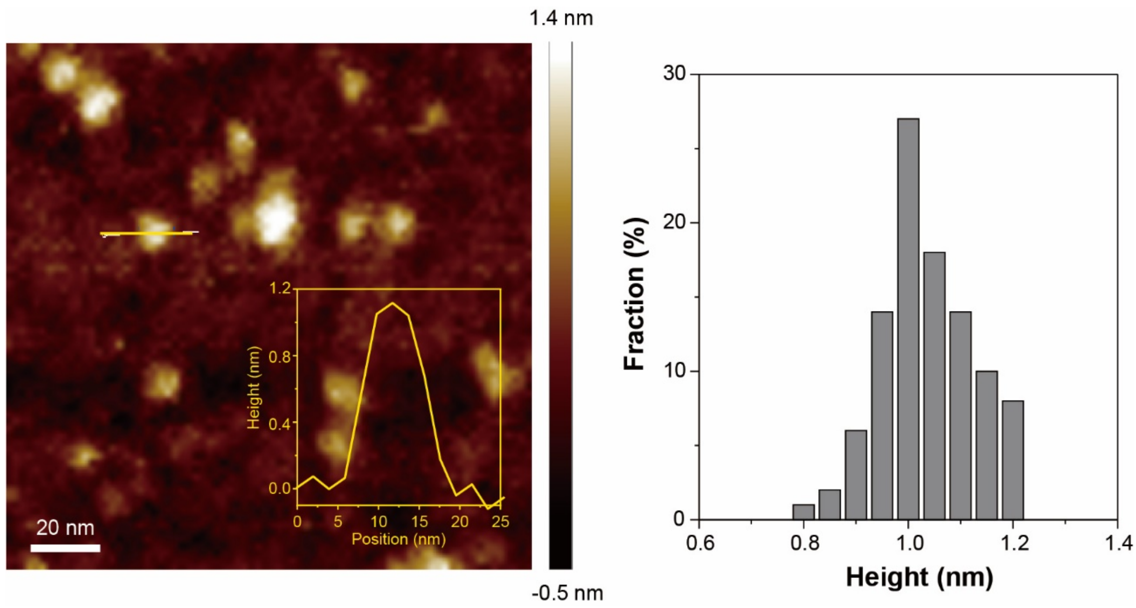

Fig. S2 Representative AFM image of N-TAGQDs. The average N-TAGQD thickness was ~1.1 nm.

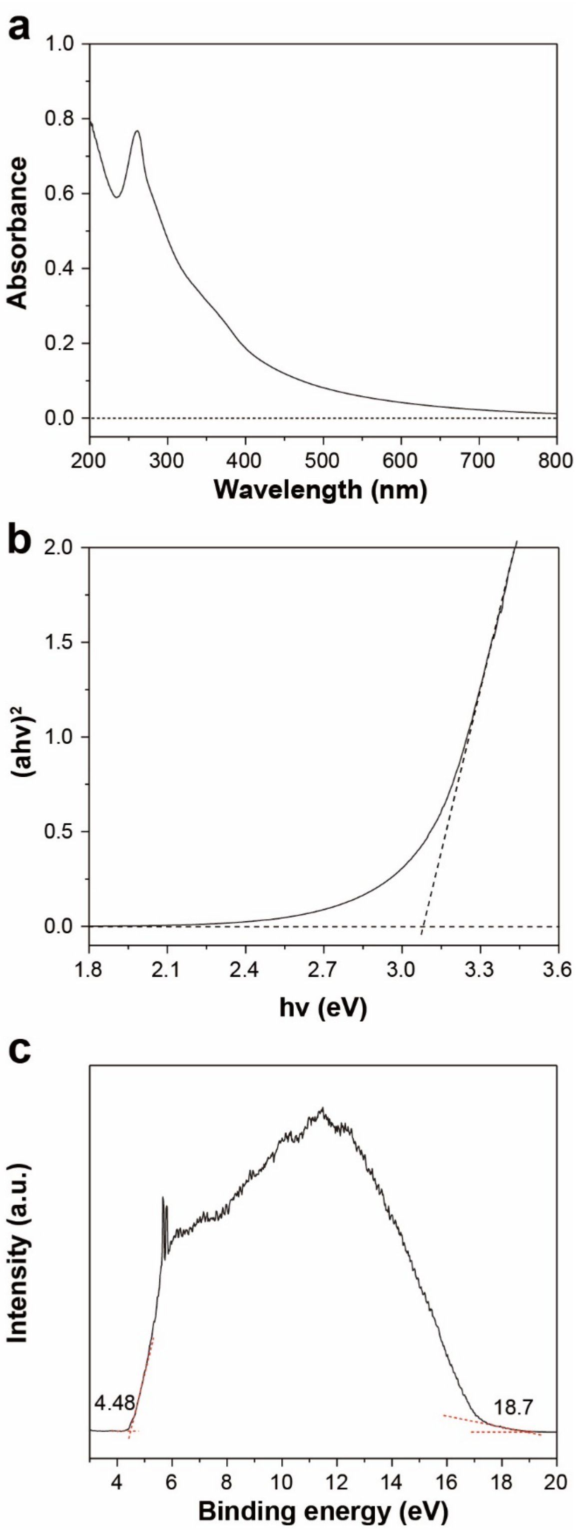

Fig. S3 (a) UV-Vis absorbance, (b) Tauc plot, and (c) UPS spectra of N-TAGQDs.

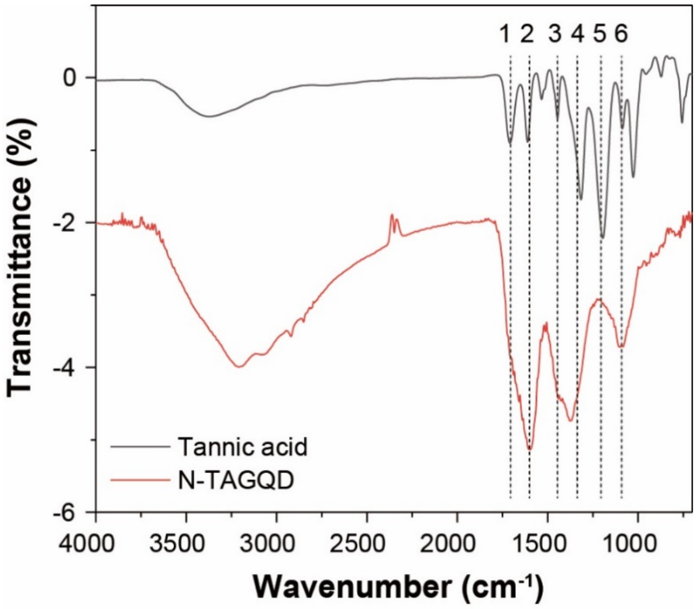

Fig. S4 FT-IR spectrum of TA and N-TAGQDs. The peaks related with TA were 1707 (1, C=O stretching), 1610 (2, C-C and C-H deformation in the benzene ring plane), 1449 (3, C=C stretch of the benzene ring, C-O stretch of phenolic groups), 1317 (4, C-O stretch and O-H deformation of phenolic groups, C-C stretch and C-H deformation in the benzene ring plane), 1196 (5, O-H deformation in the phenolic plane), and 1084 cm^{-1} (6, C-O stretch of phenolic groups). Although the intensity of C-OH peaks was reduced, those peaks related to phenolate still remained after hydrothermal reaction.

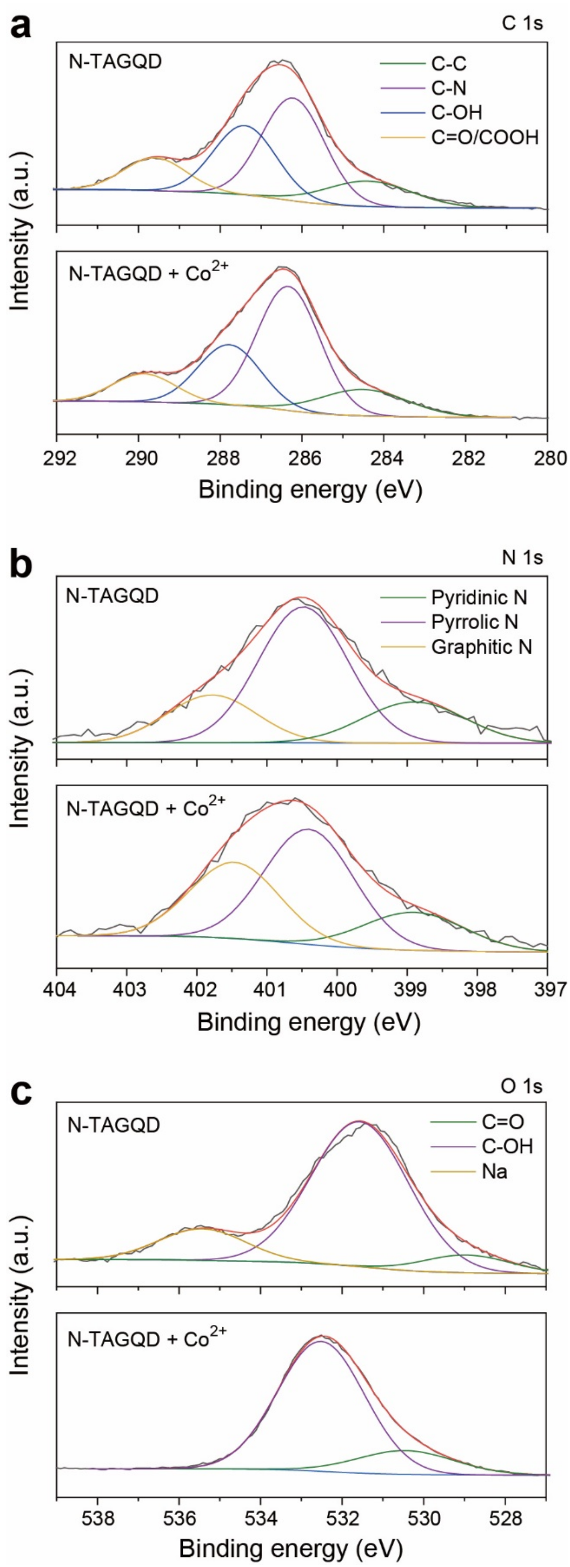

Fig. S5 High resolution XPS spectra of (a) C 1s, (b) N 1s, and (c) O 1s of N-TAGQDs and N-TAGQDs + Co^{2+} ions. After N-TAGQDs and Co^{2+} ions were mixed, the ratio of phenolic groups and pyrrolic N was reduced due to the conjugation of the abundant functional groups of N-TAGQDs and Co^{2+} ions.

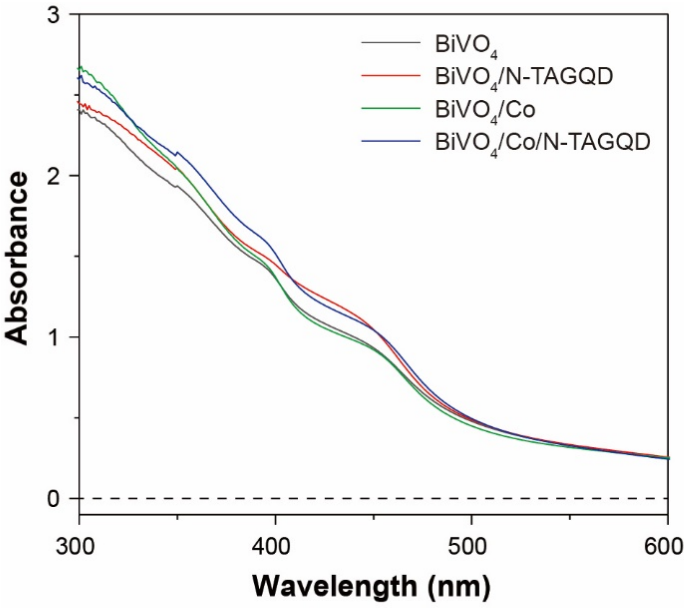

Fig. S6 UV/Vis spectra of $BiVO_4$, $BiVO_4$/N-TAGQD, $BiVO_4$/Co, and $BiVO_4$/Co/N-TAGQD.

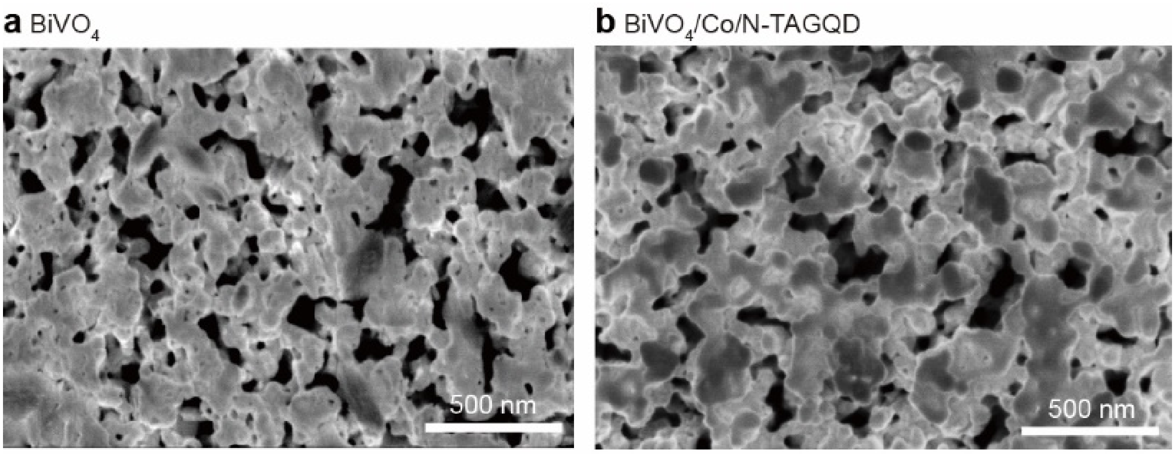

Fig. S7 SEM images of (a) $BiVO_4$ and (b) $BiVO_4$/Co/N-TAGQD.

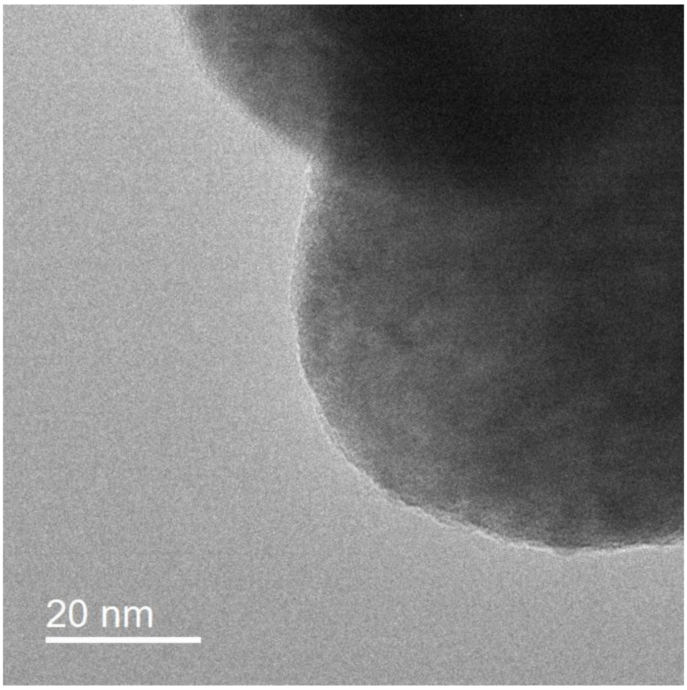

Fig. S8 TEM image of $BiVO_4$/N-TAGQD.

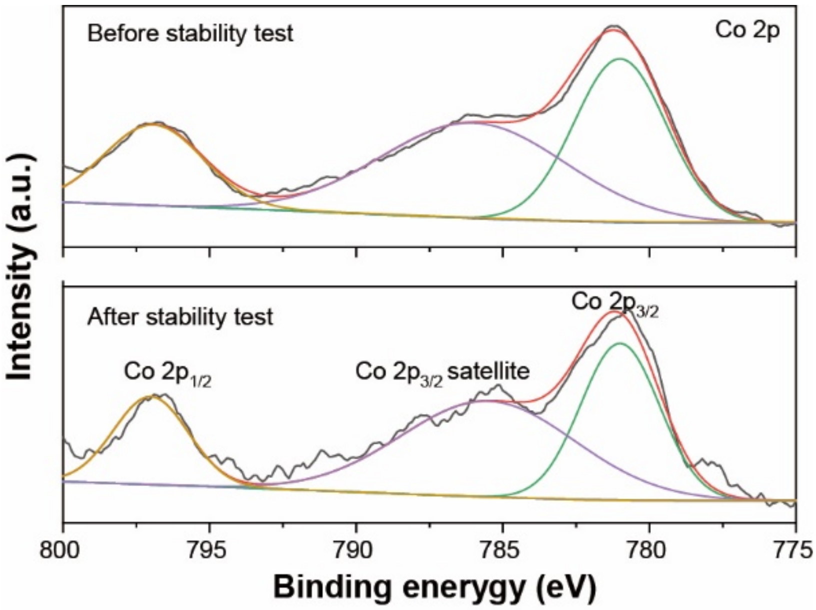

Fig. S9 High-resolution Co 2p XPS spectra of $BiVO_4$/Co/N-TAGQD before and after stability test. The content of Co^{2+} was 2.41 wt%. Three peaks at 780.7, 785.9, and 796.6 eV correspond to Co 2p3/2, Co 2p3/2 satellite, Co 2p1/2 peaks (the Co $2p_{1/2}$ satellite signal is not assigned due to its overlap with the $BiVO_4$ signal).

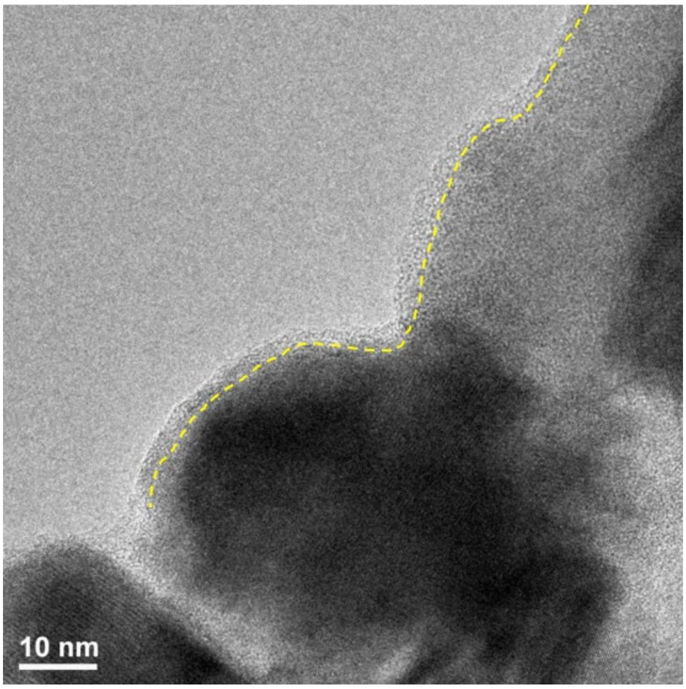

Fig. S10 TEM image of $BiVO_4$/Co/N-TAGQD after stability test for 2 h.

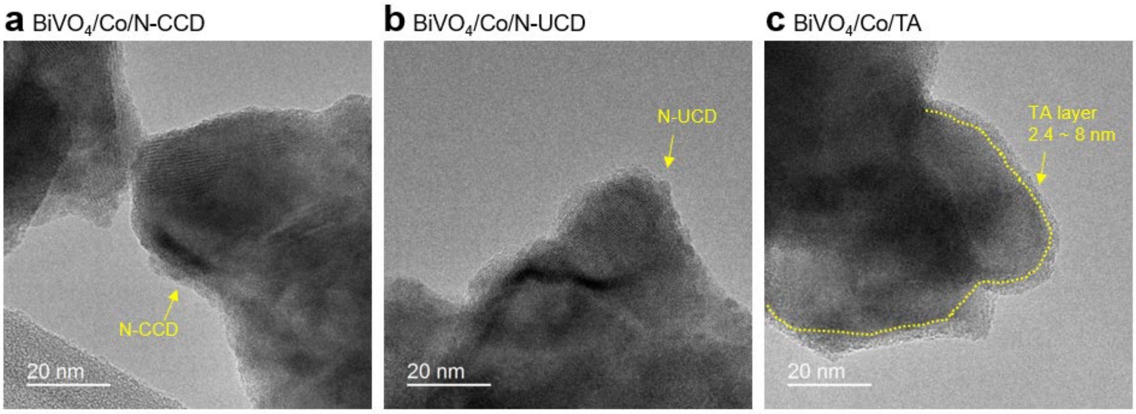

Fig. **S11** TEM images of (a) $BiVO_4$/Co/N-UCD, (b) $BiVO_4$/Co/N-CCD, and (c) $BiVO_4$/Co/TA.

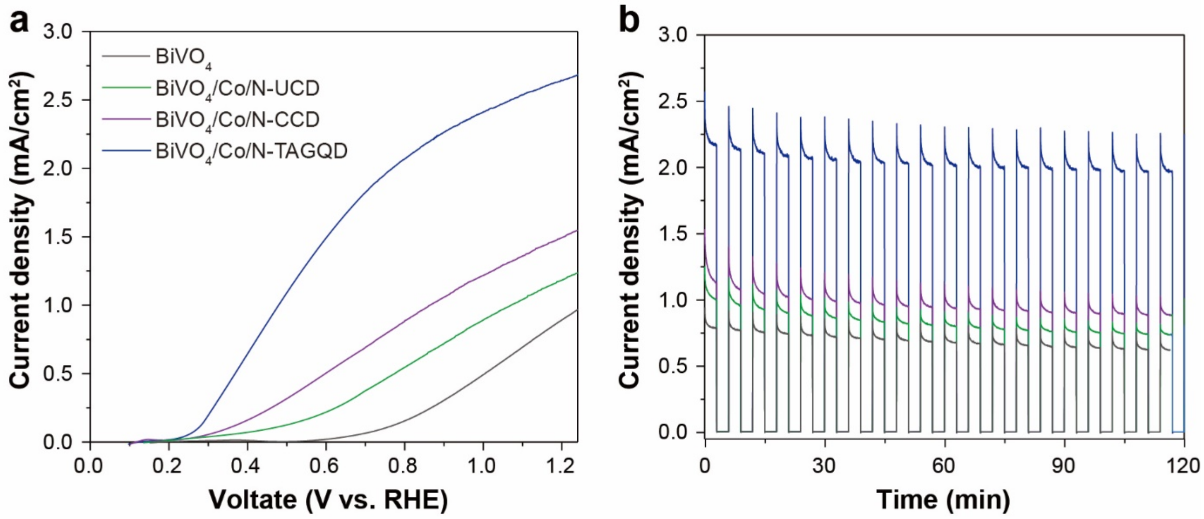

Fig. S12 (a) PEC performance of $BiVO_4$, $BiVO_4$/Co/N-UCD, $BiVO_4$/Co/N-CCD, and $BiVO_4$/Co/N-TAGQD photoanodes under simulated solar irradiation in 0.1 M phosphate buffer (pH 7.0). Scan rate: 10 mV/s. (b) Chronoamperometry curves of $BiVO_4$, $BiVO_4$/Co/N-UCD, $BiVO_4$/Co/N-CCD, and $BiVO_4$/Co/N-TAGQD collected at 1.23 V *vs*. RHE with the chopped light.

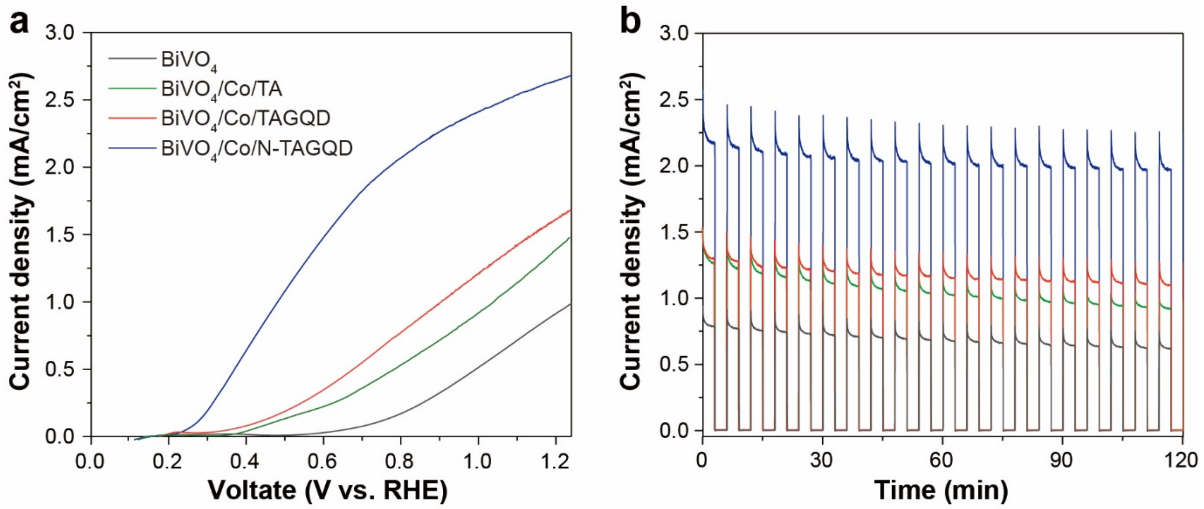

Fig. S13 (a) PEC performance of $BiVO_4$, $BiVO_4$/Co/TA, $BiVO_4$/Co/TAGQD, and $BiVO_4$/Co/N-TAGQD photoanodes under simulated solar irradiation in 0.1 M phosphate buffer (pH 7.0). Scan rate: 10 mV/s. (b) Chronoamperometry curves of $BiVO_4$, $BiVO_4$/Co/TA, $BiVO_4$/Co/TAGQD, and $BiVO_4$/Co/N-TAGQD collected at 1.23 V *vs*. RHE with chopped light.

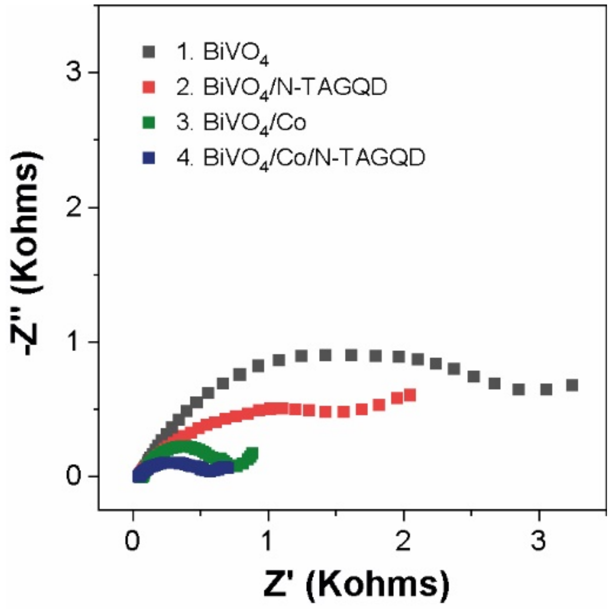

Fig. S14 Nyquist plot of (1) $BiVO_4$, (2) $BiVO_4$/N-TAGQD, (3) $BiVO_4$/Co, and (4) $BiVO_4$/Co/N-TAGQD photoanodes at 0.6 V vs. RHE under light irradiation.

Table S1 The fitting parameters obtained from EIS analysis at 0.6 V vs. RHE.

No.	Photoanode	R_s (Ω cm^{-2})	C_{sc} (F cm^{-2})	R_{bulk} (Ω cm^{-2})	C_{ss} (F cm^{-2})	R_{ct} (Ω cm^{-2})
1	$BiVO_4$	61.34	1.34e-5	444.4	3.87e-5	2007
2	$BiVO_4$/N-TAGQD	48.88	1.20e-5	269.5	8.28e-5	1159
3	$BiVO_4$/Co	73.11	1.10e-5	220.6	5.93e-5	382
4	$BiVO_4$/Co/N-TAGQD	42.12	1.06e-5	191.6	9.98e-5	232

Table S2 The fitting parameters obtained from the Bode plots in Figure 3b.

Photoanode	Charge transfer		Charge transport	
	Phase angle (°)	**Log f (Hz)**	**Phase angle (°)**	**Log f (Hz)**
$BiVO_4$	47.46	-0.077	31.80	1.76
$BiVO_4$/N-TAGQD	49.72	-0.001	19.36	2.37
$BiVO_4$/Co	27.23	0.425	28.37	1.90
$BiVO_4$/Co/N-TAGQD	6.92	0.892	25.96	2.47

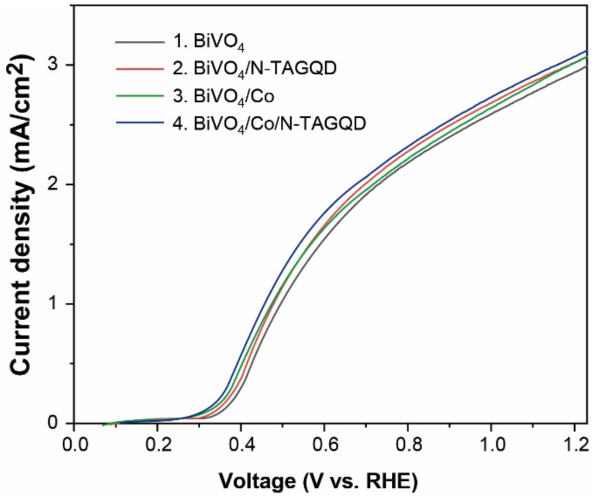

Fig. S15 LSV curves measured in the presence of electron donor (Na_2SO_3): (1) $BiVO_4$, (2) $BiVO_4$/N-TAGQD, (3) $BiVO_4$/Co, and (4) $BiVO_4$/Co/N-TAGQD.

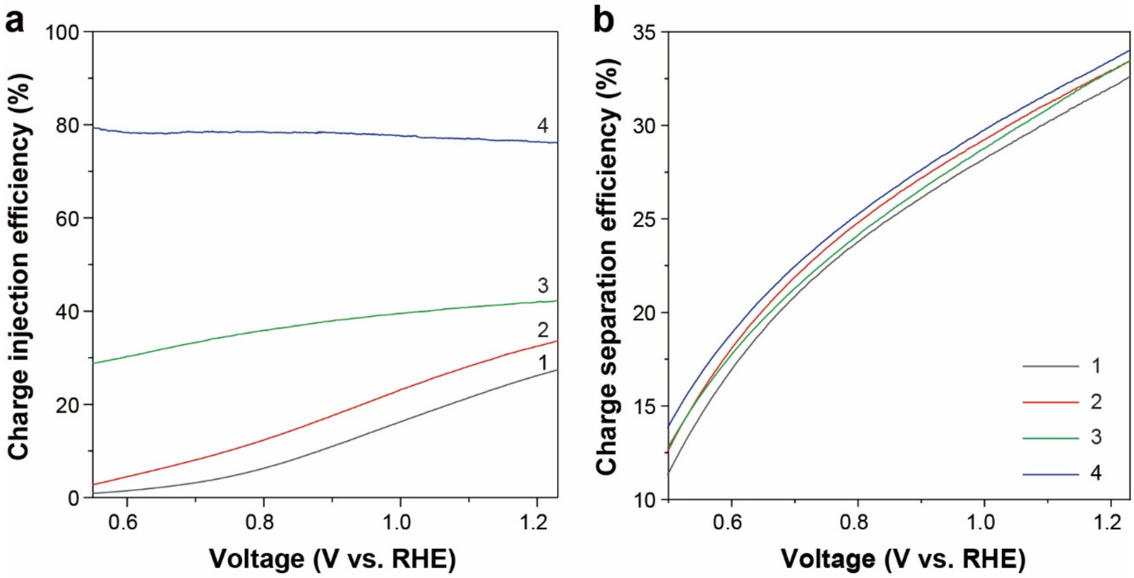

Fig. S16 (a) Charge injection efficiency and (b) charge separation efficiency of (1) $BiVO_4$, (2) $BiVO_4$/N-TAGQD, (3) $BiVO_4$/Co, and (4) $BiVO_4$/Co/N-TAGQD.

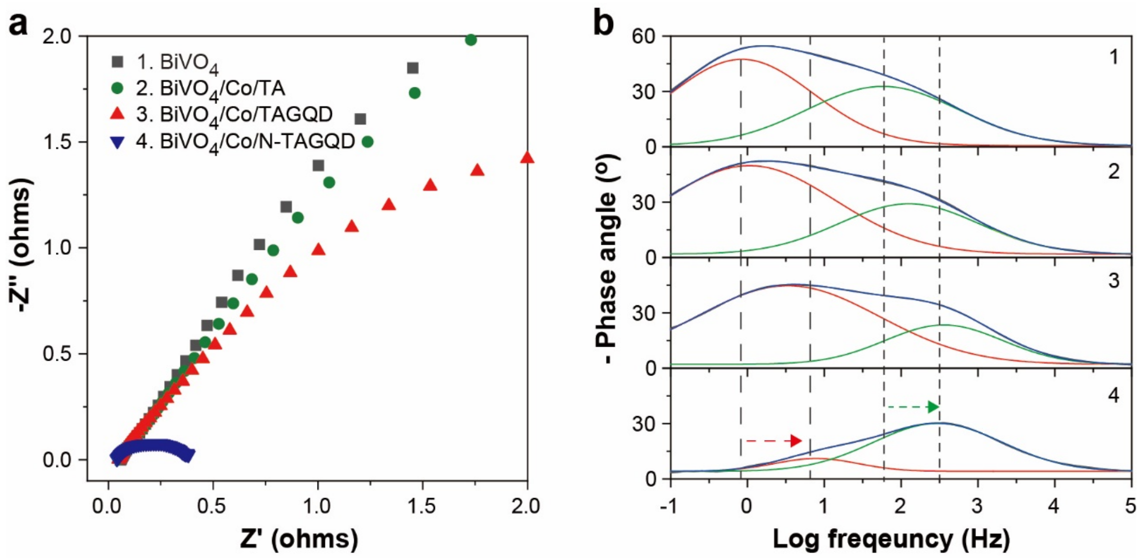

Fig. S17 EIS (a) Nyquist and (b) Bode plot analyses of $BiVO_4$, $BiVO_4$/Co/TA, $BiVO_4$/Co/TAGQD and $BiVO_4$/Co/N-TAGQD measured at 0.4 V *vs*. RHE under simulated solar irradiation in 0.1 M phosphate buffer (pH 7.0).

Table S3 The fitting parameters obtained from EIS and Bode plots.

EIS plots					
Photoanode	**R_s (Ω cm^{-2})**	**C_{sc} (F cm^{-2})**	**R_{bulk} (Ω cm^{-2})**	**C_{ss} (F cm^{-2})**	**R_{ct} (Ω cm^{-2})**
$BiVO_4$	55.38	1.77e-5	355.4	8.50e-5	5651
$BiVO_4$/N-TAGQD	49.19	1.39e-5	269.6	1.14e-4	3929
$BiVO_4$/Co	50.01	1.50e-5	245.9	8.55e-5	912
$BiVO_4$/Co/TA	53.04	1.52e-5	327.2	9.81e-5	4147
$BiVO_4$/Co/TAGQD	48.39	1.77e-5	330.4	1.02e-4	2669
$BiVO_4$/Co/N-TAGQD	42.86	5.40e-6	121.6	6.70e-4	181

Bode plots				
	Charge transfer		**Charge transport**	
Photoanode	**Phase angle (°)**	**Log f (Hz)**	**Phase angle (°)**	**Log f (Hz)**
$BiVO_4$	47.46	-0.077	31.80	1.76
$BiVO_4$/N-TAGQD	49.72	-0.001	19.36	2.37
$BiVO_4$/Co	27.23	0.425	28.37	1.90
$BiVO_4$/Co/TA	47.92	0.261	27.26	2.09
$BiVO_4$/Co/TAGQD	42.56	0.528	21.28	2.56
$BiVO_4$/Co/N-TAGQD	6.92	0.892	25.96	2.47

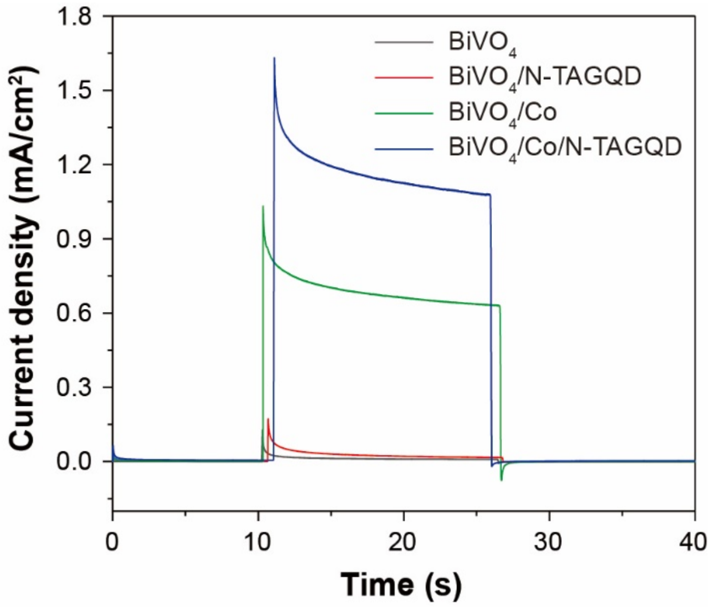

Fig. S18 Chronoamperometry graphs of $BiVO_4$, $BiVO_4$/N-TAGQD, $BiVO_4$/Co, and $BiVO_4$/Co/N-TAGQD photoanodes with chopped light at 0.6 V *vs*. RHE.

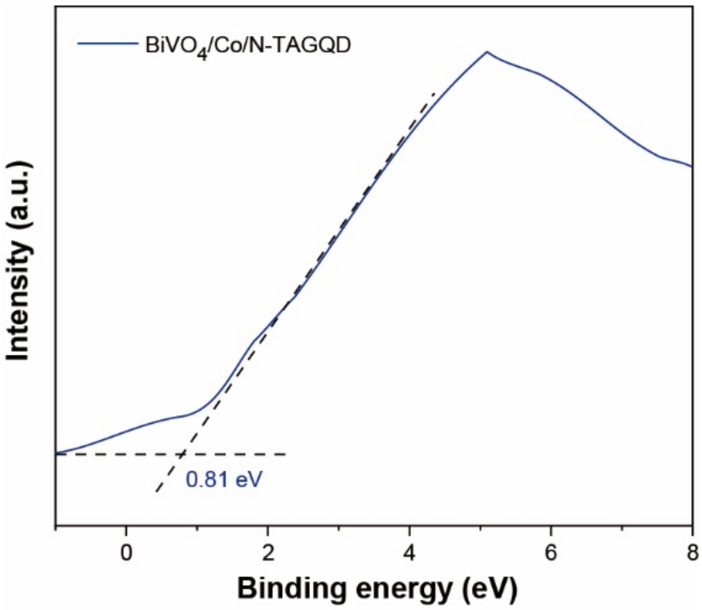

Fig. S19 XPS of $BiVO_4$/Co/N-TAGQD photoanodes for investigation of the position of valence band maximum (VBM).

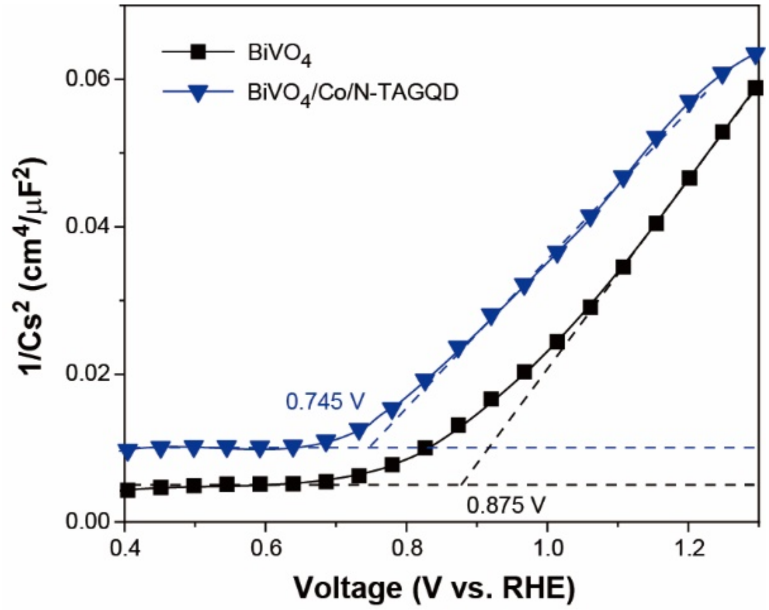

Fig. S20 Mott-Schottky plot (M-S plot) of $BiVO_4$, and $BiVO_4$/Co/N-TAGQD photoanodes under dark condition in 0.10 M phosphate buffer (pH 7.0).